# A Lightweight Approach for On-the-Fly Reflectance Estimation

Kihwan Kim[1] Jinwei Gu[1] Stephen Tyree[1] Pavlo Molchanov[1] Matthias Nießner[2] Jan Kautz[1]
[1]NVIDIA [2]Technical University of Munich
http://research.nvidia.com/publication/reflectance-estimation-fly

## Abstract

*Estimating surface reflectance (BRDF) is one key component for complete 3D scene capture, with wide applications in virtual reality, augmented reality, and human computer interaction. Prior work is either limited to controlled environments (e.g., gonioreflectometers, light stages, or multi-camera domes), or requires the joint optimization of shape, illumination, and reflectance, which is often computationally too expensive (e.g., hours of running time) for real-time applications. Moreover, most prior work requires HDR images as input which further complicates the capture process. In this paper, we propose a lightweight approach for surface reflectance estimation directly from* 8*-bit RGB images in real-time, which can be easily plugged into any 3D scanning-and-fusion system with a commodity RGBD sensor. Our method is learning-based, with an inference time of less than 90ms per scene and a model size of less than 340K bytes. We propose two novel network architectures, HemiCNN and Grouplet, to deal with the unstructured input data from multiple viewpoints under unknown illumination. We further design a loss function to resolve the color-constancy and scale ambiguity. In addition, we have created a large synthetic dataset, SynBRDF, which comprises a total of* 500*K RGBD images rendered with a physically-based ray tracer under a variety of natural illumination, covering* 5000 *materials and* 5000 *shapes. SynBRDF is the first large-scale benchmark dataset for reflectance estimation. Experiments on both synthetic data and real data show that the proposed method effectively recovers surface reflectance, and outperforms prior work for reflectance estimation in uncontrolled environments.*

## 1. Introduction

Capturing scene properties in the wild, including its 3D geometry and surface reflectance, is one of the ultimate goals of computer vision, with wide applications in virtual reality, augmented reality, and human computer interaction. While 3D geometry recovery has achieved high accuracy, especially with recent RGBD-based scanning-and-fusion approaches [7, 22, 33], surface reflectance estimation still remains challenging. At one extreme, most of the fusion methods assume Lambertian reflectance and recover surface texture only. At the other extreme, most of the prior work on surface BRDF (bidirectional reflectance distribution function) estimation [14, 20, 19] aims to recover the full 4D BRDF function, but are often limited to controlled, studio-like environments (e.g., gonioreflectometers, light stages, multi-camera domes, planar samples).

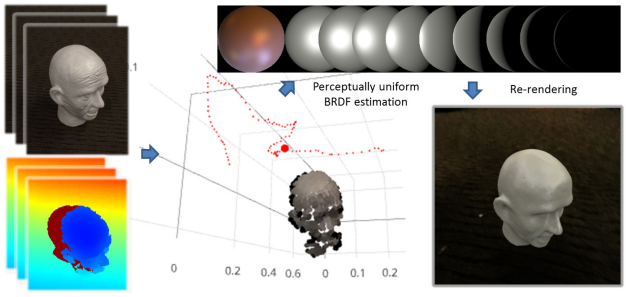


(a) (b) (c)

Figure 1. Overview of our method: we take RGBD image sequences as inputs (a). During a reconstruction process, each view contributes voxels as an observation. In (b), we visualize the color of visible voxel samples from a specific view (red circle among red dots indicating locations of other views). These samples from all views are evaluated through either HemiCNN (Sec. 3.3.1) or Grouplet networks (Sec. 3.3.2) to estimate the BRDF in real time. In (c), we show a rendered image with predicted BRDF and captured lighting and shape. More examples are shown in Sec. 4.

Recently, a few methods [35, 18, 27, 26, 30, 17, 1] were proposed to recover surface reflectance in uncontrolled environments (e.g., unknown illumination or shape) by utilizing statistical priors on natural illumination and/or BRDF. These methods formulate the inverse rendering problem as a joint, alternative optimization among shape, reflectance, and/or lighting. Despite their accuracy, these methods are computationally quite expensive (e.g., hours or days of running time and tens of gigabytes of memory consumption) and are often run in a post-process rather than a real-time setting. Moreover, these methods often require high-resolution HDR images as input, which further complicates the capturing process for real-time or interactive applications on consumer-grade mobile devices.

In this paper, we propose a lightweight and practical approach for surface reflectance estimation directly from 8-bit RGB images in real-time. The method can be easily plugged into any 3D scanning-and-fusion system with a commodity RGBD sensor and enables physically-plausible renderings at novel lighting/viewing conditions, as shown in Fig. 1. Similar to prior work [35, 18], we use a simplified BRDF representation and focus on estimating surface albedo and gloss rather than full 4D BRDF function. Our method is learning-based, with an inference time of less than 90ms per scene and a model size of less than 340K bytes.

In order to deal with unstructured input data (e.g., each surface point can have a different number of observations due to occlusions) in the context of neural networks, we propose two novel network architectures – HemiCNN and Grouplet. HemiCNN projects and interpolates the sparse observations onto a 2D image, which enables the use of standard convolutional neural networks. Grouplet learns directly from random samples of observations and uses multilayer perception networks. Both networks are also designed to be lightweight in both inference time and model size for real-time applications on consumer-grade mobile devices. In addition, since the illumination is unknown, we have designed a novel loss function to resolve the color-constancy and scale ambiguity (i.e., only given input images, we do not know whether surfaces are reddish or the lighting is reddish, or whether surfaces are dark or the lighting is dim). *To the best of our knowledge, this is the first lightweight, real-time approach for surface reflectance estimation in the wild.*

We also created a large-scale synthetic dataset — SynBRDF— for reflectance estimation. SynBRDF covers 5000 materials randomly sampled from OpenSurfaces [3], 5000 shapes from ScanNet [6], and a total of 500K RGBD images (both HDR and LDR) rendered from multiple viewpoints with a physically-based ray tracer under 20 natural environmental illumination conditions, making it an ideal benchmark dataset for complete image-based 3D scene reconstruction.

Finally, we incorporated the proposed approach with RGBD scanning-and-fusion for complete 3D scene capture (see Sec. 4 and Fig. 8). We trained our networks with SynBRDF and directly applied the trained models on real data captured with a commodity RGBD sensor. Experiments on both synthetic data and real data show that the proposed method effectively recovers surface reflectance and outperforms prior work for surface reflectance estimation in uncontrolled environments.

## 2. Related Work

**Surface Reflectance Estimation in Uncontrolled Environments** Most prior work in this direction formulate the inverse rendering problem as a joint optimization among the three radiometric ingredients—lighting, geometry, and reflectance—from observed images. Barron et al. [1] assume Lambertian surfaces and optimize all the three components. Others [30, 8, 17, 9] optimize reflectance and illumination with known 3D geometry, either from motion or based on statistical priors on natural illumination and materials. Recently, Wu et al. [35] and Lombardi et al. [18] proposed to jointly estimate lighting, reflectance, and 3D shape from a RGBD sensor, even in the presence of interreflection. Chandraker et al. [5] investigated the theoretical limits of material estimation from a single image. Despite their effectiveness, these methods solve complicated optimization problems iteratively, which is computationally too expensive for real-time applications (e.g., hours of running time). As the optimization relies heavily on the parametric forms of statistical priors, these methods generally require good initialization and HDR images as input. In contrast, our proposed method is a lightweight and practical approach that can estimate surface reflectance directly from 8-bit RGB images on-the-fly, which is suitable for real-time applications.

**Material Perception and Recognition** Our work is also inspired from prior work on material perception and recognition from images. Pellacini et al. [28] designed a perceptually-uniform representation of the isotropic Ward BRDF model [32], and Wills et al. [34] extend to data-driven models with measured reflectance. Fores et al. [11] studied the metrics used for BRDF fitting [23]. Fleming et al. [10] found that natural illumination is key for the perception of surface reflectance. Bell et al. [3] released a large dataset—OpenSurfaces—with annotated surface appearance from real-world materials. These prior works inspired us in designing the regression loss and creating a synthetic dataset for training. For learning-based material recognition, Liu et al. [16] proposed a Bayesian approach based on a bag of visual features. Bell et al. [4] used CNNs (convolutional neural networks) for material recognition from material context input. Recently, Wang et al. [31] proposed a CNN-based method for material recognition from light field images. These prior work shows neural networks are capable of learning discriminative features for material perception from images.

**Reflectance Maps Estimation and Intrinsic Image Decomposition** Intrinsic image decomposition aims to factor an input image into a shading-only image and a reflectance-only image. Recently, CNNs has been successfully employed for intrinsic image decomposition [15, 21] from a single image. Bell et al. [2] proposed a dense CRF-based method and released a large intrinsic image dataset generated by crowdsourcing. Zhou et al. [36] used deep learning to infer data-driven priors from sparse human annotations. Rematas et al. [29] used CNNs to estimate re-

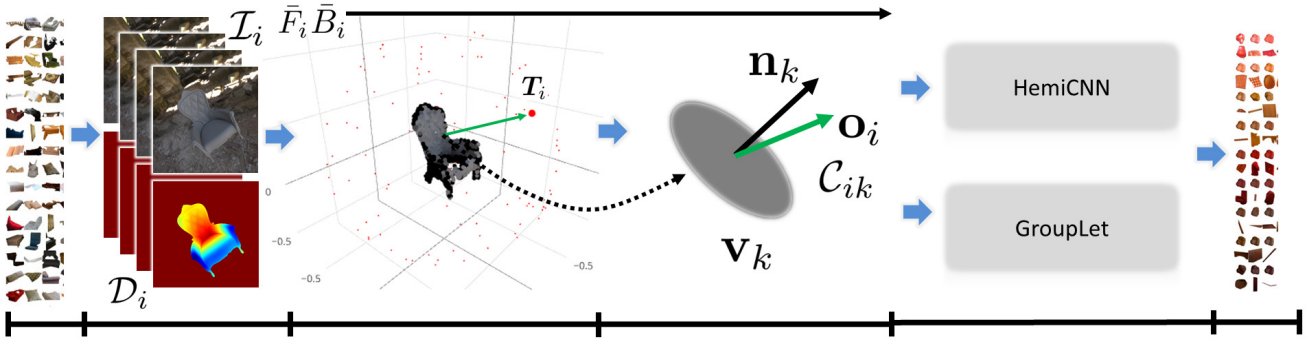


Figure 2. **Overview of our framework: (a)** BRDF examples from OpenSurface [3], **(b)** Input image $\mathcal{I}_i$ and depth $\mathcal{D}_i$ streams. Integrated volume is shown in **(c)**, where the colors shown from $i$th view $\mathcal{I}_i$ (the red circle with pose $\boldsymbol{T}_i$) are visualized. Small red dots refer to the locations of other views. **(d)** shows the data that we extract from each voxel $\mathbf{v}_k$ for training: normal $\mathbf{n}_k$, observation vector $\mathbf{o}_i$ (the green arrow), and color values $\mathcal{C}_{ik}$ from the observation $\mathcal{I}_i$ at the voxel $\mathbf{v}_k$. In **(e)**, these measurements together with color statistics ($\bar{F}_i$ and $\bar{B}_i$) are fed into one of the two networks, HemiCNN (Sec. 3.3.1) and Grouplet (Sec. 3.3.2) for BRDF estimation.

flectance maps (defined as 2D reflectance under fixed, unknown illumination) from a single image. These methods recover only the illumination-dependent reflectance map, while our method estimates the full BRDF that enables rendering under novel illumination and viewing conditions.

## 3. Method

Our goal is to develop a module for real-time surface reflectance estimation that can be plugged into any 3D scanning-and-fusion methods for 3D scene capture, with potential applications in VR/AR. In this paper, we make a significant step towards this goal, and propose two novel networks for *homogeneous* surface reflectance estimation from RGBD image input.

### 3.1. Framework and Reflectance Model

Our framework takes as input RGBD image/depth sequences from a commodity depth sensor (Fig. 1). We denote RGB color observation as $\mathcal{C} : \Omega_{\mathcal{C}} \rightarrow \mathbb{R}^3$, images with $\mathcal{I} : \Omega_{\mathcal{I}} \rightarrow \mathbb{R}^3$ and depth maps with $\mathcal{D} : \Omega_{\mathcal{D}} \rightarrow \mathbb{R}$. The $N$ acquired RGBD frames consist of RGB color images $\mathcal{I}_i$, and depth maps $\mathcal{D}_i$ (with frame index $i \in 1 \dots N$). We also denote the absolute camera poses $\boldsymbol{T}_i = (\boldsymbol{R}, \boldsymbol{t}) \in \mathrm{SE}(3)$, $\boldsymbol{t} \in \mathbb{R}^3$ and $\boldsymbol{R} \in \mathrm{SO}(3)$ of the respective frames, which is computed from standard volume-based pose-estimation algorithm [7].[1] As shown in Fig. 2, the input $\mathcal{I}_i$, and $\mathcal{D}_i$ are aligned and integrated into a 3D volume $\mathcal{V}$ with signed-distance fusion [24], from which we extract voxels $\mathbf{v}_k \in \mathcal{V}$ ($k \in 1 \dots M$) that contain observed color $\mathcal{C}_{ik}$ from the corresponding view $\mathcal{I}_i$, its surface normal $\mathbf{n}_k$, and camera orientation $\mathbf{o}_i$, see Fig. 2(d). Additionally, we compute the color statistics for each view by simply taking the average of foreground and background pixels in $\mathcal{I}_i$, denoted as $\bar{F}_i$ and $\bar{B}_i$, respectively. We will discuss these further in Sec. 3.2.

For the representation of surface reflectance, similar to prior work [35, 18], we choose a parametric BRDF model—the isotropic Ward BRDF model [32]—for two reasons: (1) the Ward BRDF model has a simple form but is representative for a wide variety of real-world materials [23], and (2) prior studies [28, 34] on BRDF perception are based on the Ward BRDF model. Specifically, the isotropic Ward BRDF model is given by:

$$f(\omega_i, \omega_o; \Theta) = \frac{\rho_d}{\pi} + \rho_s \cdot \frac{\exp\left(-\tan^2 \theta_h / \alpha^2\right)}{4\pi\alpha^2 \sqrt{\cos\theta_i \cos\theta_o}}, \qquad (1)$$

where $\omega_i = (\theta_i, \phi_i)$ and $\omega_o = (\theta_o, \phi_o)$ are the incident and viewing directions, $\theta_h$ is the half angle, and $\Theta = (\rho_d, \rho_s, \alpha)$ is the parameter to be estimated.

An equivalent, but perceptually-uniform representation of the Ward BRDF model was proposed in [28], where the diffuse albedo $\rho_d$ is converted from RGB to CIE Lab colorspace, $(L, a, b)$, and the gloss is described by variables $c$, the contrast of gloss, and $d$, the distinctness of gloss. Variables $c$ and $d$ are related to the BRDF parameters by [28]:

$$c = \sqrt[3]{\rho_s + \rho_d/2} - \sqrt[3]{\rho_d/2}, \quad d = 1 - \alpha. \qquad (2)$$

Thus, an alternative representation for the BRDF parameters is $\Theta = (L, a, b, c, d)$.

Our problem is thus formulated as follows. *Given a set of voxels from any 3D scanning-and-fusion pipeline, $\{\mathbf{v}_k\} = \{\{\mathcal{C}_{ik}, \mathbf{o}_i\}, \mathbf{n}_k\}$, we estimate the optimal BRDF parameters $\Theta$ with neural networks.* Two problems need to be solved for learning. First, what is a good loss function that can resolve the color constancy and scale ambiguities due to unknown illumination? For example, just from input images, we cannot tell whether the material is reddish or the illumination is reddish, or whether the material

[1] During training, we randomly generated poses for rendering scenes.

| Name | $\mathbf{E_d}(\Theta, \hat{\Theta})$ |
|---|---|
| $\text{RMSE}_1$ | $\|\|\rho_d - \hat{\rho_d}\|\|^2 + \|\|\rho_s - \hat{\rho_s}\|\|^2 + \|\|\alpha - \hat{\alpha}\|\|^2$ |
| $\text{RMSE}_2$ | $\|\|\text{Lab} - \hat{\text{Lab}}\|\|^2 + \lambda_g \|\|\text{cd} - \hat{\text{cd}}\|\|^2$ |
| Cubic Root | $\sqrt[3]{\int_{\omega_i,\omega_o} \|\|f(\omega_i,\omega_o;\Theta) - f(\omega_i,\omega_o;\hat{\Theta})\|\| \cos\theta_i d\omega_o d\omega_o}$ |

Table 1. Three options for the distance function $E_d(\Theta, \hat{\Theta})$ for BRDF estimation. $\text{RMSE}_1$ and $\text{RMSE}_2$ are root mean squared error using $\Theta = (\rho_d, \rho_s, \alpha)$ and $\Theta = (L, a, b, c, d)$, respectively, where the latter is the sum of the perceptual color difference and the perceptual gloss difference ($\lambda_g = 1$) [28]. Cubic Root is the cosine-weighted $\ell_2$-norm of the difference of two 4D BRDF functions, inspired by BRDF fitting [23, 11].

is dark or the illumination is dim. Second, the input data is unstructured — different voxels have different numbers of observations due to occlusion. What is a good network architecture for such unstructured input data? We address these two problems in the following sections.

### 3.2. Design of the Loss Function

A key part for network training is an appropriate loss function. Prior work [23, 11] has shown that the commonly-used $\ell_2$ norm (i.e., MSE) is not optimal for BRDF fitting. We design the following loss:

$$J = E_d(\Theta, \hat{\Theta}) + \lambda E_c(\hat{\Theta}, \{\mathcal{C}_{ik}\}), \tag{3}$$

where $E_d(\cdot,\cdot)$ measures the discrepancy between the estimated BRDF parameters and the ground truth and $E_c(\cdot,\cdot)$ is a regularization term which relates the estimated reflectance $\hat{\Theta}$ with observed image intensities $\{\mathcal{C}_{ik}\}$. $E_c$ aims to resolve the aforementioned scale and color constancy ambiguities and is weighted by $\lambda = 0.01$ in all our experiments

Table (1) lists three options for $E_d(\Theta, \hat{\Theta})$ implemented in this paper. $\text{RMSE}_1$ and $\text{RMSE}_2$ are the root mean squared error with $\Theta = (\rho_d, \rho_s, \alpha)$ and $\Theta = (L, a, b, c, d)$, respectively, where the latter is the sum of the perceptual color difference and the perceptual gloss difference ($\lambda_g = 1$) [28]. Cubic Root is inspired from BRDF fitting [23, 11], which is a cosine weighted $\ell_2$-norm of the difference between two 4D BRDF functions.

For $E_c$, we use the color statistics computed for each view, $\bar{F}_i$ and $\bar{B}_i$, to approximately constrain the estimation of $\rho_d$ and $\rho_s$. Specifically, $E_c$ is derived based on the rendering equation [13] as

$$E_c = \sum_i ||(\rho_d + \rho_s) \cdot \bar{B}_i^\gamma - \bar{F}_i^\gamma||^2, \tag{4}$$

where $\bar{F}_i$ and $\bar{B}_i$ are the average image intensity of the foreground and background regions of the $i$-th input image $I_i$, $\gamma = 2.4$ is used to convert the input 8-bit RGB images to linear images; see the Appendix for a detailed derivation. Even though Eq. (4) is only an approximation of the rendering equation, it imposes a soft constraint on the scale and color cues for the BRDF estimation. We found it quite effective for working with real data (see Fig. 8).

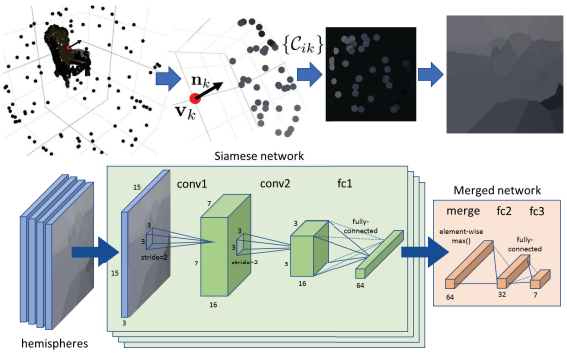


Figure 3. Details of HemiCNN. *Top row:* generating a voxel hemisphere image, from the sparse 3D set of the observations $\{\mathcal{C}_{ik}\}$ of voxel $v_k$ to a dense 2D hemisphere representation. *Bottom row:* the HemiCNN siamese convolutional neural network architecture.

### 3.3. Network Architectures

As shown in Fig. 2, our input data is unstructured because the observations $\mathcal{C}_{ik}$ for each voxel $\mathbf{v}_k$ are irregular, sparse samples on the 2D slice of the 4D BRDF. Different voxels may have different numbers of observations due to occlusion. In order to feed the unstructured input data into networks for learning, we propose two new neural network architectures. One is called Hemisphere-based CNN (HemiCNN) which projects and interpolates the sparse observations onto a 2D image, enabling the use of standard convolutional neural networks. The other architectures, called Grouplet, learns directly from randomly sampled observations and uses a multilayer perceptron network. Both networks are also designed to be lightweight in both inference time per scene ($\leq$90ms) and model size ($\leq$340KB).

#### 3.3.1 Hemisphere-based CNN (HemiCNN)

For HemiCNN, as shown in the top row of Fig. 3, the RGB observations $\{\mathcal{C}_{ik}\}$ of voxel $\mathbf{v}_k$ are projected onto a unit sphere centered at the sample voxel $\mathbf{v}_k$. The unit sphere is rotated so the positive $z$-axis is aligned with the voxel's surface normal $\mathbf{n}_k$. Observations $\{\mathcal{C}_{ik}\}$ on the positive hemisphere (i.e., $z > 0$) are projected onto the 2D $x$-$y$ plane. Finally, a dense 2D image, denoted a sample hemisphere image, is generated using nearest-neighbor interpolation among the projected observations.

A siamese convolutional neural network is used to predict BRDF parameters from a collection of $N$ sample hemisphere images, one for each of a representative set of voxels, e.g., chosen by clustering on voxel positions or surface normals. As shown in Fig. 3, in the first of two stages the siamese convolutional network operates on each sample hemisphere image individually to produce a vector representation, after which the representations are merged across

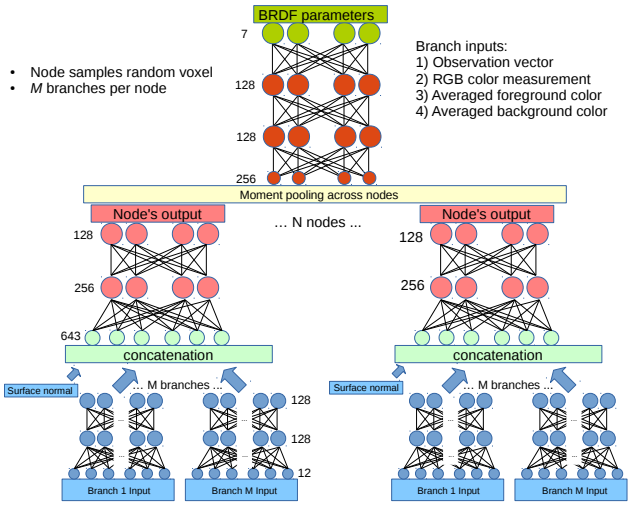


Figure 4. The Grouplet model for BRDF estimation relies on aggregating results from a set of weak regressors (nodes). Each node operates on a randomly sampled voxel from the object. $M$ branches form the input to a node; each samples randomly from a set of observations. Intermediate representation from multiple nodes are combined by a moment pooling layer. BRDF parameters are regressed from the output of the moment pooling layer.

the $N$ samples (i.e., voxels) by computing an element-wise maximum. The network includes two convolutional layers, each with 16 sets of $3 \times 3$ filters with ReLU activations, a single $2 \times 2$ max-pooling layer, and a single fully-connected layer with 64 neurons. After aggregating the $N$ feature vectors with an elementwise-maximum, we use a fully-connected layer with 32 neurons, followed by tanh activation, and a final fully-connected layer to produce the BRDF prediction. In most experiments with HemiCNN, we set $N = 25$. The model size is 56KB and the average inference time is 16ms per scene.

#### 3.3.2 Sampling-based Network (Grouplet)

The second proposed network architecture is called Grouplet (Fig. 4). Unlike HemiCNN, where we transform sparse observations to 2D images to use standard convolution layers, Grouplet directly operates on each observation $\mathcal{C}_{ik}$ for each voxel $\mathbf{v}_k$. Grouplet relies on aggregating results from a set of weak regressors called *nodes*. Each node estimates an intermediate representation of the BRDF parameters of a single voxel ($\mathbf{v}_k$) from $M$ randomly sampled observations $\Gamma_k = \{\mathcal{C}_{1k}, \cdots, \mathcal{C}_{Mk}\}$, as shown in Fig. 4. A different subsets of observations is sampled for each voxel. Each observation from $\Gamma_k$ is processed by a two-layer multilayer perceptron (MLP) with 128 neurons per layer, called a *branch*. Inputs to each branch are observed color ($\mathcal{C}_{ik}$), viewing direction ($\mathbf{o}_i$), averaged foreground color ($\bar{F}_i$) and averaged background color ($\bar{B}_i$).

Next, the output of $M$ branches are concatenating together with the voxel's surface normal ($\mathbf{n}_k$). This vector is processed by another two-layer MLP with 256 and 128 neurons in the layers, the output of which is the intermediate representation of the BRDF parameters. During BRDF estimation, we operate on $N$ voxels, each of which is processed by different nodes with shared weights. To combine the intermediate representations computed from several voxels, we use a moment pooling operator that is invariant to the number of nodes. We pool with the first and second central moments which represent expected value and variance of the intermediate representation across nodes. The output of the pooling operator is a 256-dimensional pooled representation.

The final part of the network estimates the BRDF parameters from the pooled representation by another MLP with two hidden layers of 128 neurons each, and one final output layer. All layers throughout the model use hyperbolic tangent activation functions except for the last output layer.

Grouplet is able to work with any number of nodes due to the use of pooling operators. It also does not require that the number of nodes be the same during training and testing. However, the order of the $M$ observations in the branch networks is important. We found the best results by sorting observations by the cosine distance between the observation vector ($\mathbf{o}_i$) and the voxel's surface normal ($\mathbf{n}_k$). For BRDF estimation, Grouplet is applied in two forms, *Grouplet-fast* and *Grouplet-slow*, with $N = 20$ and $N = 354$ voxels, respectively. Each constructs $M = 5$ nodes per voxel. The average inference time is 5ms for Grouplet-fast and 90ms for Grouplet-slow. The model size for both Grouplet-fast and Grouplet-slow is 339KB. Unless otherwise noted, Grouplet refers to Grouplet-slow.

For both HemiCNN and GroupLet, we set $\lambda_g = 1$ and explore a range of $\lambda$, finding $0.1 \leq \lambda \leq 1$ to be a reasonable range. We train HemiCNN using RMSProp with learning rate 0.0001 and 100K minibatches. For Grouplet training, we use stochastic gradient descent with fixed learning rate 0.01 and momentum 0.9 for 13K minibatches.

### 3.4. SynBRDF: A Large Benchmark Dataset

Deep learning requires a large amount of data. Yet, for BRDF estimation, it is extremely challenging to obtain a large dataset with measured BRDF data due to the complex settings required for BRDF acquisition [19, 17]. Moreover, while there are quite a few recent works for 3D shape recovery and reflectance estimation in the wild [17, 27, 35], we are not aware of a large-scale, benchmark dataset with ground-truth shape, reflectance, and illumination.

With these motivations, we created SynBRDF which is, to our knowledge, the first large-scale, synthetic benchmark dataset for BRDF estimation. SynBRDF covers 5000 materials randomly sampled from OpenSurfaces [3], 5000 shapes randomly sampled from ScanNet [6], and a total

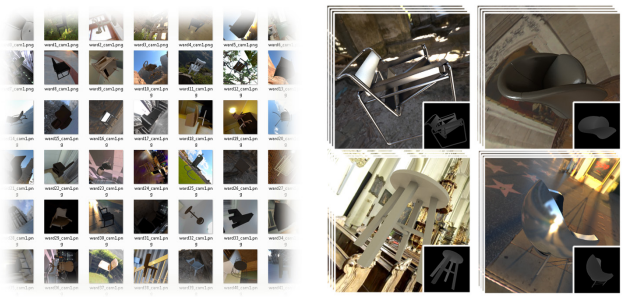

Figure 5. **SynBRDF**: (Left) Thumbnails of the first frame of each example (each contains 100 different observations), (Right) Some examples with depth map (insets)

of 500K RGB and depth images (both HDR and LDR) rendered from multiple viewpoints with a physically-based raytracer [12], under variants of 20 natural environmental illumination maps. SynBRDF thus has ground truth for 3D shape, BRDF, illumination, and camera pose, making it an ideal benchmark dataset for evaluating image-based 3D scene reconstruction and BRDF estimation algorithms. As shown in Fig. 5, each scene is labeled with ground truth Ward BRDF parameters (Eq. 1 and 2). For more flexible evaluation that allows other types of rendering (e.g., global illumination) for the same scene, we will also provide the 90K XML files that indicate the original OpenSurface materials and contain the variations of environmental and object model settings. We believe this dataset will be valuable for further study in this direction.

In our experiments, we used SynBRDF for training and evaluation. We randomly chose 400 from the total 5000 scenes as a holdout test set, and the remaining 4600 scenes for training. For real data experiments, we directly applied the trained models without any domain adaptation.

| Network | Loss | RMSE | User Rank |
|---|---|---|---|
| Grouplet | $\text{RMSE}_1 + E_c$ | 0.455 | 1 |
| Grouplet | $\text{RMSE}_1$ | 0.432 | 2 |
| HemiCNN | $\text{RMSE}_2$ | 0.564 | 3 |
| HemiCNN | CubeRoot | 0.439 | 4 |
| HemiCNN | $\text{RMSE}_1$ | 0.419 | 5 |
| HemiCNN | $\text{CubeRoot} + E_c$ | 0.583 | 6 |
| Grouplet | $\text{RMSE}_2$ | 0.457 | 7 |

Table 2. Average RMSE (w.r.t ground truth BRDF parameters) on the test set of SynBRDF and the rank of user preferences from a perceptual study of rendered materials. Among the variants of our proposed method, we list the top seven methods based on the results of the user study. In general these provide most plausible results among all testing data (see results in Fig. 7 and Fig. 9). Note that RMSE ranking is not always consistent with the ranking of user study. Further, as shown in Fig. 8, CubeRoot+$E_c$ provides most plausible results for the real data. Additional evaluations are found in the Supplementary Material.

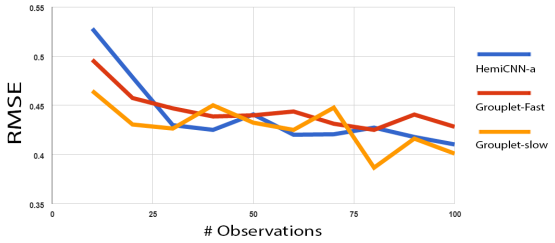


Figure 6. Error versus the number of observations for three methods: HemiCNN (blue), Grouplet-fast (20 voxel samples, red), and Grouplet-slow (354 voxel samples, orange). A larger set of observations yields noticeably improved predictions for all three methods, but begins to saturate around 30. The common *scan-and-fuse* method does not always guarantee a rich coverage of observations.

## 4. Experimental Results

We evaluated multiple variants of the proposed networks, changing the loss function $E_d$ and BRDF representations as described in Sec 3.1. In Sec. 4.1, we evaluate these settings on SynBRDF, showing quantitatively and qualitatively that several combinations give accurate predictions on our synthetic dataset. In Sec. 4.2, we compare with prior work [17]. Finally in Sec. 4.3, we demonstrate the proposed methods within the KinectFusion pipeline for complete 3D scene capture with real data.

### 4.1. Results on Synthetic Data

We evaluated all variants of the proposed methods on the test set of SynBRDF. Evaluating the quality of BRDF estimation is challenging [11]—perceived quality often varies with the illumination, 3D shape, and even display settings. Estimates with the lowest RMSE error on the BRDF parameters are not necessarily the best for visual perception. Thus, in addition to computing the RMSE with respect to the ground truth BRDF parameters, we also conducted a user study. We randomly chose 10 materials from the test set, and rendered the BRDF predictions for each material under (a) natural illumination and (b) moving point light sources. The rendered images are similar to Fig. 7. We then asked 10 users to rank the methods on each material based on the perceptual similarity between the ground truth and the images rendered from each method.

Table 2 lists the top seven methods based on average user score, together with the RMSE w.r.t ground truth BRDF parameters.[2] (Additional evaluation results are provided in the Supplementary Material.) We found the RMSE ranking is not always consistent with the ranking of the user study. Adding the regularization term $E_c$ can improve the ranking (e.g., Grouplet-$\text{RMSE}_1$-$E_c$), while the choice of

[2]RMSE is computed after normalization of the BRDF parameters to zero mean and unit standard deviation, based on the mean and standard deviation of the training set. Thus a random prediction (with the same statistics) will have RMSE $\approx 1.0$.

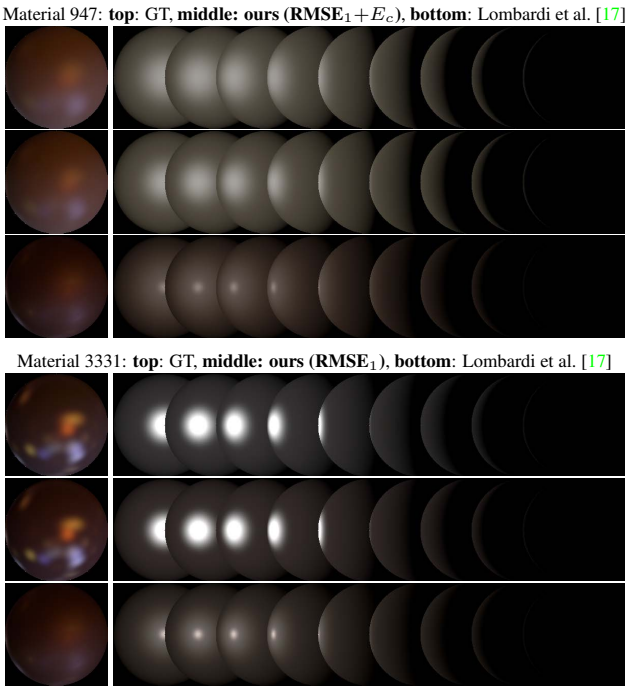


Figure 7. Comparison with Lombardi et al. [17]: ours (middle row for each example) is closer to the ground truth example (top row) even under varying lighting.

$E_d$ has mixed effect on performance. We find that the $\Theta = (L, a, b, c, d)$ BRDF representation provides more accurate estimation of gloss (e.g., HemiCNN-RMSE$_2$). Also, HemiCNN seems able to obtain better estimate for the gloss, while Grouplet estimates the diffuse albedo better.

Fig. 9 shows three random examples of BRDF estimation. We show the rendered images under natural illumination with the ground truth BRDF, as well as the estimated BRDF from two variants of our proposed method. Qualitatively, the BRDF estimations accurately reproduce the color and gloss of the surface materials.

### 4.2. Comparison with [17]

As mentioned previously, it is difficult to compare with prior work on BRDF estimation in the wild [27, 35], given the lack of code and common datasets for comparison. Lombardi et al. [17] is the only method with released codes. Strictly speaking, it is not a direct apples-to-apples comparison, because Lombardi et al. [17] requires a single image and a precise surface normal map as input and estimates both DSBRDF and lighting, while our methods take multiple RGB-D images as input and estimate the Ward BRDF. Moreover, Lombardi et al. [17] takes about 3 minutes to run, while our methods are real-time ($\leq$ 90ms). Nevertheless, Lombardi et al. [17] is the only available option for comparison, and both its input requirements and running time are similar to ours. For comparison, we randomly chose two materials from SynBRDF, rendered a sphere image under natural illumination, and used it (together with the sphere normal map) as the input for [17]. Fig. 7 shows the comparison. Our proposed method closely matches the ground truth and outperforms [17].

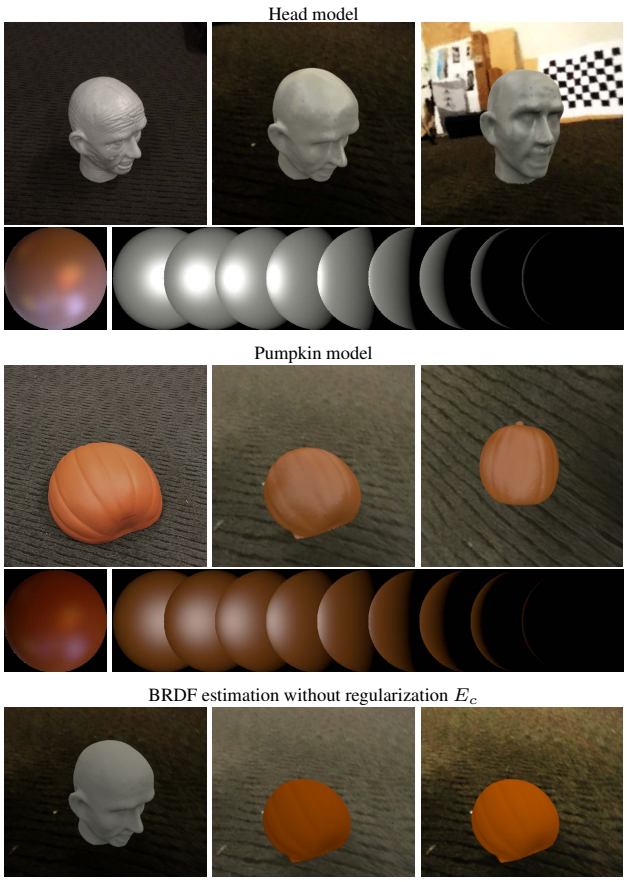


Figure 8. **Real data evaluation:** For both examples in the top two sections, head and pumpkin, *top-left* is the input (real) scene, *top-middle* shows the rendered scene with estimated BRDF parameters, *top-right* shows a different rendered view of the same scene, *bottom-left* shows a rendered sphere with the estimated BRDF, and *bottom-right* shows rendered spheres with varying point lighting. Grouplet and HemiCNN with CubeRoot + $E_c$ were used for the head and pumpkin examples, respectively. The bottom section shows three rendered views from methods trained without regularization $E_c$ (Eq. 4).

### 4.3. Results on Real Data

Previously, in Sec. 1 and Sec. 3.2, we discussed the potential issues of scale ambiguity present in real-world data, due in part to our use of commodity RGBD camera output rather than HDR videos. As expected, the regularization (Eq. 4) plays an important role in achieving correct results, as illustrated in Fig. 8. Notice that the result with the regularization better captures brightness as well as plausible gloss. Additional views of the real examples are shown in the supplementary video.

## 5. Conclusions and Limitations

In this paper, we proposed a lightweight and practical approach for surface reflectance estimation directly from 8-bit RGB images in real-time. The method can be plugged into 3D scanning-and-fusion systems with a commodity RGBD sensor for scene capture. Our approach is learning-based, with the inference time less than 90ms per material and model size less than 340K bytes. Compared to prior work, our method is a more feasible solution for real-time applications (VR/AR) on mobile devices. We proposed two novel network architectures, HemiCNN and Grouplet, to handle the unstructured measured data from input images. We also designed a novel loss function that is both perceptually-based and able to resolve the scale ambiguity and color-constancy ambiguity for reflectance estimation. In addition, we also provided the first large-scale synthetic data set (SynBRDF) as a benchmark dataset for training and evaluation for surface reflectance estimation in uncontrolled environments.

Our method has several limitations that we plan to address in future work. First, our method estimates homogeneous reflectance. While GroupLet and HemiCNN can in theory operate for each voxel separately and thus could estimate spatially-varying reflectance, in practice we found using more voxels as input results in more robust estimation. One future direction is to jointly learn several basis reflectance functions and weight maps to estimate spatially-varying BRDF. Second, we use the isotropic Ward model for BRDF representation. In the future, we plan to investigate more general, data-driven models such as DS-BRDF [25] and the related perceptually-based loss [34]. Finally, we are interested in using neural networks to jointly refine both 3D geometry and reflectance estimation, and leveraging domain adaption techniques to further improve the performance on real data.

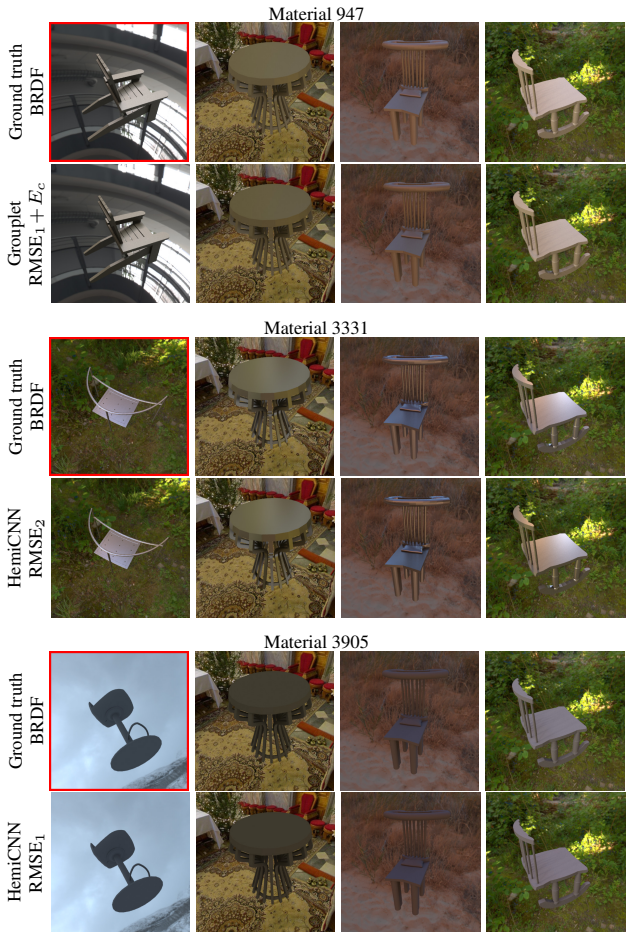


Figure 9. Qualitative results for three randomly selected materials. For each material, images in first row are rendered from ground truth BRDF, while images in the second row are rendered from the estimated BRDF using one of the methods from the list in Table 2. The ground truth image indicated with a red border is sampled from the image sequence used for inference (inputs). To demonstrate how different objects and environmental lights can change the appearance of the scene even with the same BRDF, the three images from second to fourth columns are rendered with the same BRDF but different models and lighting. More examples from different are included in the Supplementary Material.

## Appendix

**Derivation of Eq.(4)** For viewing direction $\omega_o$, the observed scene radiance $L_o$ is given by

$$L_o = \int_{\omega_i} f(\omega_i, \omega_o; \Theta) \cdot L_i \cdot \max(\cos\theta_i, 0) d\omega_i, \qquad (5)$$

where $L_i$ is the environmental illumination in the direction $\omega_i$. We simplified the above rendering equation so that all terms can be computed from the input fed into the networks. Suppose the environment illumination is uniform, i.e., $L_i = \bar{L}$, by integrating the reflected radiance from the entire hemisphere, the measured radiance is:

$$\bar{L_o} \approx (\rho_d + \rho_s)\bar{L}. \qquad (6)$$

Both $\bar{L_o}$ and $\bar{L}$ can be approximated from input images, where the average intensity of the foreground object is close to $\bar{L_o}$, and the average intensity of the background is close to $\bar{L}$. Since the input images are 8-bit images in the sRGB color space rather than linear HDR images, we need to apply an additional gamma transformation between pixel intensities and scene radiance ($\gamma = 2.4$ for sRGB). Thus, we have $\bar{L_o} \approx \bar{F}^\gamma$ and $\bar{L} \approx \bar{B}^\gamma$, where $\bar{F}$ and $\bar{B}$ are the average image intensities for the foreground and background. Putting all together, we have

$$\bar{F_i^\gamma} \approx (\rho_d + \rho_s) \cdot \bar{B_i^\gamma}, \qquad (7)$$

and thus we have the $E_c$ term in Eq.(4).

## References


[1] J. T. Barron and J. Malik. Shape, illumination, and reflectance from shading. *IEEE Trans. Pattern Anal. Mach. Intell.*, 2015. 1, 2

[2] S. Bell, K. Bala, and N. Snavely. Intrinsic images in the wild. *ACM Trans. Graph.*, 33(4):159:1–159:12, July 2014. 2

[3] S. Bell, P. Upchurch, N. Snavely, and K. Bala. Opensurfaces: A richly annotated catalog of surface appearance. *ACM Trans. Graph. (SIGGRAPH)*, 2013. 2, 3, 5

[4] S. Bell, P. Upchurch, N. Snavely, and K. Bala. Material recognition in the wild with the materials in context database. *Computer Vision and Pattern Recognition (CVPR)*, 2015. 2

[5] M. Chandraker and R. Ramamoorthi. What an image reveals about material reflectance. In *ICCV*, pages 1–8, 2011. 2

[6] A. Dai, A. X. Chang, M. Savva, M. Halber, T. Funkhouser, and M. Nießner. Scannet: Richly-annotated 3d reconstructions of indoor scenes. *http://arxiv.org/*, 2017. 2, 5

[7] A. Dai, M. Nießner, M. Zollhöfer, S. Izadi, and C. Theobalt. Bundlefusion: Real-time globally consistent 3D reconstruction using on-the-fly surface re-integration. *arXiv*, 2016. 1, 3

[8] Y. Dong, G. Chen, P. Peers, J. Zhang, and X. Tong. Appearance-from-motion: Recovering spatially varying surface reflectance under unknown lighting. *ACM Trans. Graph.*, 2014. 2

[9] R. O. Dror, E. Adelson, and A. Willsky. Estimating surface reflectance properties from images under unknown illumination. In *SPIE, Human Vision and Electronic Imaging*, 2001. 2

[10] R. W. Fleming, R. O.Dror, and E. Adelson. Real-world illumination and the perception of surface reflectance properties. *Journal of Vision*, 2003. 2

[11] A. Fores, J. Ferwerda, and J. Gu. Toward a perceptually based metric for brdf modeling. In *Twentieth Color and Imaging Conference. Los Angeles, California, USA*, pages 142–148, November 2012. 2, 4, 6

[12] W. Jakob. Mitsuba Renderer, 2010. http://www.mitsuba-renderer.org. 6

[13] J. T. Kajiya. The rendering equation. In *SIGGRAPH*, 1986. 4

[14] H. P. A. Lensch, J. Kautz, M. Goesele, W. Heidrich, and H.-P. Seidel. Image-Based Reconstruction of Spatially Varying Materials. In S. J. Gortle and K. Myszkowski, editors, *Eurographics Workshop on Rendering*, 2001. 1

[15] L. Lettry, K. Vanhoey, and L. V. Gool. Darn: A deep adversial residual network for iintrinsic image decomposition:. Arxiv. 2

[16] C. Liu, L. Sharan, R. Rosenholtz, and E. H. Adelson. Exploring features in a bayesian framework for material recognition. In *CVPR*, 2010. 2

[17] S. Lombardi and K. Nishino. Reflectance and natural illumination from a single image. In *ECCV*, pages 582–595, 2012. 1, 2, 5, 6, 7

[18] S. Lombardi and K. Nishino. Radiometric scene decomposition: Scene reflectance, illumination, and geometry from rgb-d images. In *3DV*, 2016. 1, 2, 3

[19] W. Matusik, H. Pfister, M. Brand, and L. McMillan. A data-driven reflectance model. *SIGGRAPH*, 2003. 1, 5

[20] D. McAllister. *A Generalized Surface Appearance Representation for Computer Graphics*. PhD thesis, University of North Carolina at Chapel Hill, 2002. 1

[21] T. Narihira, M. Maire, and S. X. Yu. Direct iintrinsic: Learning albedo-shading decomposition by convolutional regression. In *ICCV*, 2015. 2

[22] R. Newcombe, A. Davison, S. Izadi, P. Kohli, O. Hilliges, J. Shotton, D. Molyneaux, S. Hodges, D. Kim, and A. Fitzgibbon. KinectFusion: Real-time dense surface mapping and tracking. In *ISMAR*, 2011. 1

[23] A. Ngan, F. Durand, and W. Matusik. Experimental analysis of brdf models. In *Proceedings of the Eurographics Symposium on Rendering*, pages 117–226. Eurographics Association, 2005. 2, 3, 4

[24] M. Nießner, M. Zollhöfer, S. Izadi, and M. Stamminger. Real-time 3D reconstruction at scale using voxel hashing. *ACM Transactions on Graphics (TOG)*, 32(6):169, 2013. 3

[25] K. Nishino and S. Lombardi. Directional statistics-based reflectance model for isotropic bidirectional reflectance distribution functions. *OSA Journal of Optical Society of America A*, 28(1):8–18, 2011. 8

[26] K. Nishino and S. Lombardi. Single image multimaterial estimation. *CVPR*, pages 238–245, 2012. 1

[27] G. Oxholm and K. Nishino. Shape and reflectance estimation in the wild. *TPAMI*, 38(2):376–389, 2016. 1, 5, 7

[28] F. Pellacini, J. A. Ferwerda, and D. P. Greenberg. Toward a psychophysically-based light reflection model for image synthesis. In *Proceedings of the 27th Annual Conference on Computer Graphics and Interactive Techniques*, SIGGRAPH '00, pages 55–64, 2000. 2, 3, 4

[29] K. Rematas, T. Ritschel, M. Fritz, E. Gavves, and T. Tuytelaars. Deep reflectance maps. In *CVPR*, 2016. 2

[30] F. Romeiro and T. Zickler. Blind reflectometry. In *ECCV*, 2010. 1, 2

[31] T. Wang, J. Zhu, E. Hiroaki, M. Chandraker, A. Efros, and R. Ramamoorthi. A 4d light-field dataset and cnn architectures for material recognition. In *ECCV*, 2016. 2

[32] G. J. Ward. Measuring and modeling anisotropic reflection. In *Proceedings of the 19th Annual Conference on Computer Graphics and Interactive Techniques*, SIGGRAPH '92, pages 265–272, 1992. 2, 3

[33] T. Whelan, S. Leutenegger, R. S. Moreno, B. Glocker, and A. Davison. Elasticfusion: Dense slam without a pose graph. In *Proceedings of Robotics: Science and Systems*, Rome, Italy, July 2015. 1

[34] J. Wills, S. Agarwal, D. Kriegman, and S. Belongie. Toward a perceptual space for gloss. *ACM Trans. Graph.*, 2009. 2, 3, 8

[35] H. Wu, Z. Wang, and K. Zhou. Simultaneous localization and appearance estimation with a consumer rgb-d camera. *IEEE Trans. Visualization and Computer Graphics*, 2016. 1, 2, 3, 5, 7

[36] T. Zhou, P. Krahenbuhl, and A. A. Efros. Learning data-driven reflectance priors for intrinsic image decomposition. In *ICCV*, 2015. 2